Catalysis Today 149 (2010) 407–412

Contents lists available at ScienceDirect

Catalysis Today

journal homepage: www.elsevier.com/locate/cattod

Ni(II)–Mg(II)–Al(III) catalysts for hydrogen production from ethanol steam reforming: Influence of the activation treatments

Adriana Romero [a], Matías Jobbágy [b], Miguel Laborde [a], Graciela Baronetti [a], Norma Amadeo [a,*]

[a] Laboratorio de Procesos Catalíticos, Departamento de Ingeniería Química, Facultad de Ingeniería Ciudad Universitaria, (1428) Buenos Aires, Argentina
[b] INQUIMAE, Facultad de Ciencias Exactas y Naturales, Universidad de Buenos Aires, Pabellón II, Ciudad Universitaria, (1428) Buenos Aires, Argentina

ARTICLE INFO

Article history:
Available online 29 July 2009

Keywords:
Bioethanol
Hydrogen production
LDH
Ni catalyst
Reforming

ABSTRACT

The effect of the Ni(II)–Mg(II)–Al(III) layered double hydroxide (LDH) activation conditions over the surface and bulk composition and the catalytic performance in ethanol steam reforming (ESR) is studied. Ternary oxides were prepared by thermal decomposition of LDHs synthesized using the homogeneous precipitation method with urea. Catalyst precursor is submitted to two different activation treatments: calcinations at 400, 500, 600 and 700 °C with subsequent reduction at 720 °C, or direct reduction at 720 °C. The samples were characterized by sorptometry, H_2 chemisorption, ICP chemical analysis, thermogravimetric analysis, X-ray diffraction, X-ray photoelectronic spectroscopy and temperature programming reduction. The catalysts obtained by calcination at 600 °C and then reduction at 720 °C and those directly reduced at 720 °C showed the better performance in ESR. The precursor submitted to a proper thermal treatment develops, through a decoration-demixing process, a Ni(II)-poor spinel-type shell onto NiO domains.

Published by Elsevier B.V.

1. Introduction

During the last centuries, human civilization solved the energy supply problem mainly on the bases of fossil sources of carbon and hydrocarbons and the associated technologies. The XXI century scenario claims for alternative sources and technologies. Most of the chemical based alternatives consider hydrogen as an efficient energetic vector since it directly transforms chemical reactions into electric energy by means of fuel cells technology, releasing steam as the only product. However, hydrogen non-contaminant character depends on the nature of the raw material used as source. In this sense, steam reforming of ethanol, obtained from biomass, offers a true green alternative for H_2 production, due to its inherent renewable character, low toxicity (unlike methanol) and the fact that it can be obtained virtually sulphide-free [1,2]. Ethanol has relatively high hydrogen content and in presence of water, is capable of producing 6 mol of H_2 per mol of ethanol:

$$C_2H_5OH + 3H_2O \rightarrow 2CO_2 + 6H_2 \quad (1)$$

From a thermodynamic viewpoint, reforming reaction is highly favourable, but it competes with multiple side reactions [1,3] and in general, the outflow from the reactor contents a wide range of liquids and gaseous products. Different catalytic systems have been proved to be effective with variable hydrogen selectivity's [1–11]. Ni catalysts have been widely utilized in reforming of hydrocarbons because it promotes the rupture of the C–C bonds, achieving high activity [11–14]. Noble-metal-catalysts (Rh, Pt, and Pd) also present high activity and selectivity [9], however their high cost limits their high-scale-use, in contrast to nickel based ones. In order to prevent undesired carbon formation, ternary Ni(II)–Mg(II)–Al(III) oxides were proposed, where the presence of Mg(II) disfavour this undesired product [15].

Concerning to the preparation of such catalysts, many reports suggested the use of carbonate layered double hydroxides (LDHs) as suitable precursors, since such compounds present, after an activation treatment, Ni metal nanoparticles highly dispersed within a high surface area oxidic matrix [16,17]. Mixed oxides obtained by thermal decomposition of defined crystalline precursors offer a more rational and reproducible procedure.

Melo and Morlanés [16] and Dung et al. [18] studied the effect of the thermal treatments on the performance of the catalysts obtained from LDH precursor. They used hydrocarbon steam reforming and acetonitrile hydrogenation, respectively, as reaction test. In this paper we analyze the influence of the thermal treatments on the performance of the same catalyst using ethanol steam reforming as reaction test and also considering the effect of direct reduction of the precursor on the catalyst performance.

The aim of this work is to explore the chemical and structural evolution of a crystalline Ni(II)–Mg(II)–Al(III) LDH under different

* Corresponding author. Fax: +54 11 4576 3241.
E-mail addresses: norma@di.fcen.uba.ar, normaamadeo@yahoo.com.ar (N. Amadeo).

0920-5861/$ – see front matter. Published by Elsevier B.V.
doi:10.1016/j.cattod.2009.05.026

activation procedures. The effect of activation conditions over the surface and bulk properties and the catalytic performance towards the reforming reaction of ethanol is discussed.

2. Experimental

2.1. Synthesis and characterization

Mother solutions of Al(III), Ni(II) and Mg(II) nitrates (0.5 mol/l, each) were prepared dissolving $Al(NO_3)_3{\cdot}9H_2O$, $Ni(NO_3)_2{\cdot}6H_2O$ and $Mg(NO_3)_2{\cdot}6H_2O$ in distilled water, respectively. Catalyst's precursor were prepared by homogeneous precipitation method based on urea hydrolysis [19,20], for which solutions containing urea–Ni(II)–Mg(II)–Al(III) were aged at 90 °C during 24 h in PP bottles. The reaction was quenched submitting the bottles into ice-bath. The precipitated solid is centrifuged, washed with cold distilled water and dried in stove at 70 °C, getting the precursor denominated HT. Total concentrations for the starting solutions of urea and cations [Ni(II) + Mg(II) + Al(III)] were 0.5 mol/l and 5.0×10^{-2} mol/l, respectively. Initial molar ratio of [Ni(II) + Mg(II)]/Al(III) and Mg(II)/Ni(II) were 3 and 1, respectively.

The HT precursor undergoes different activation treatments, obtaining the catalysts: ex-HT-CXR (where X denotes calcination temperature in °C; and R means "reduction") and ex-HT-R. In particular, the samples ex-HT-CXR are obtained in two steps, first the HT precursor is calcined at X temperature, and then, in a second step, the calcined sample undergoes a reduction to obtain the ex-HT-CXR catalyst. The other activation process involves a single step in which HT precursor is directly reduced, to obtain the ex-HT-R catalyst. Calcination and reduction protocols are as follows: during the calcination step, the sample is submitted to a heating ramp in air (100 ml/min) of 10 °C/min until reaching the corresponding X temperature, which is keeping for 5 h. Under direct reduction treatment, we use a heating ramp of 10 °C/min until 720 °C, holding such temperature for 2 h, in pure hydrogen flux of 100 ml/min.

Samples were characterized by sorptometry (S_{BET}), H_2 chemisorption, ICP chemical analysis, thermogravimetric analysis (TGA), powder X-ray diffraction (PXRD), X-ray photoelectron spectroscopy (XPS) and temperature programmed reduction (TPR).

BET surface area was obtained in a Micromeritics ASAP 2020 equipment. Reduced Ni area was evaluated by H_2 static volumetric chemisorption measurements. Ni metallic area was estimated assuming a Ni/H = 1 stoichiometry and that a Ni atom occupies 6.45 Å^2. Solid composition was analyzed in a Sequential Plasma Spectrometer ICP-AES Shimadzu 1000 III. Thermogravimetric studies were carried out in a Shimadzu TGA-51H equipment, using a heating ramp of 10 K/min in air flux of 50 cm^3/min or hydrogen flux of 100 cm^3/min. Solids were characterized by XRD in a Siemens D 5000 equipment (radiation Cu Kα). XPS analysis was carried out in a multi-technical system (SPECS) which has a hemispheric analyzer PHOIBOS 150 operating in fix analyzer transmission mode (FAT). Spectra were acquired with step energy of 30 eV, using Mg Kα radiation X-ray source operated at 200 W and 12 kV. Work pressure in analysis chamber was lower than 5×10^{-9} mbar. Spectra quantification was made by CasaXPS Software [21] using the analyzer's transmission function appropriated values of the Scofield factors. Curves were deconvolucionated by Gaussian and Lorentzian-type functions and Shirley-type background no-lineal subtraction. Binding energy values were corrected using the aluminium oxide Al 2p line in the calcined sample at 74.3 eV as reference [22].

TPR experiments were performed in a quartz reactor heated in electric oven with a thermal conductivity detector, using an amount of sample of 30 mg, N_2/H_2 flow of 100 ml/min (molar composition 98/2%) and a heating ramp of 5 °C/min in the range of 20–900 °C. Previously, the precursor was calcined at 350 °C during 0.5 h in air flux (100 ml/min) in order to avoid anion reduction (carbonates, nitrates) to occur simultaneously with the metallic cation reduction. Previous runs with different amounts of pure CuO were carried out in order to quantify the detector signal.

2.2. Catalytic performance

Experimental equipment used for catalytic evaluation consists of a quartz tubular reactor (Ø = 9.2 mm) heated in electric oven at the reaction temperature, which is monitored by a thermocouple placed inside the reactor. The ethanol and water feed is pumped with a syringe pump and evaporated before the entrance of the reactor, using nitrogen as carrier. Hydrogen (product from reforming) is added to this vaporized current to inhibit probable carbon formation and finally it is diluted with argon at the entrance of the reactor. Inlet and outlet composition analysis were carried out by GC in Agilent Technologies 6890N equipment.

Typical operative conditions are the following: catalyst mass: 6 mg for calcined samples and 8 mg for HT samples (in order to compensate the inherent mass loss of HT sample); reaction temperature: 550 °C, inlet ethanol molar fraction: 0.0195, inlet H_2 molar fraction: 0.0160, water/ethanol molar ratio: 5.5, inert flow: 350 ml/min. The catalyst was diluted 1:10 with an inert solid. These operation conditions prevent mass transfer limitations and guarantee isothermal conditions, no carbon formation and ethanol conversions less than 100%, which enables a proper catalytic activity evaluation.

3. Results and discussion

Chemical analysis for HT sample, reports a composition that responds to the following formula: $Ni_{0.51}Mg_{0.14}Al_{0.35}(OH)_2(CO_3)_{0.17}{\cdot}nH_2O$. Fig. 1 shows PXRD pattern for HT sample; the main interbasal reflections (0 0 3), (0 0 6), in addition to the characteristic (1 1 0) and (1 1 3) reflections close to $2\theta = 60$; indicate the presence of crystalline carbonate-intercalated Hydrotalcite-like structure [23]. Additionally, there is no evidence of Ni(II), Mg(II) or Al(III) pure crystalline phase segregation [24].

Thermal decomposition (TGA), whether in oxidizing or reducing atmosphere, for HT sample is shown in Fig. 2. Both evolutions are similar and occur in two steps, typical for LDHs [25]. At low

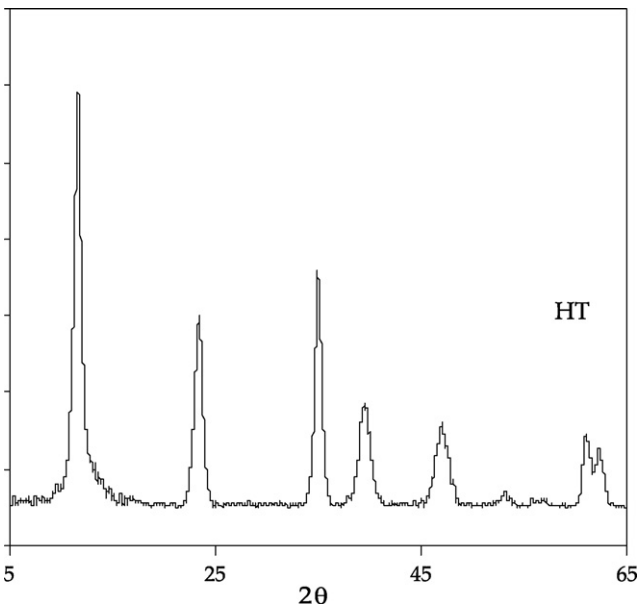

Fig. 1. PXRD pattern for HT precursor.

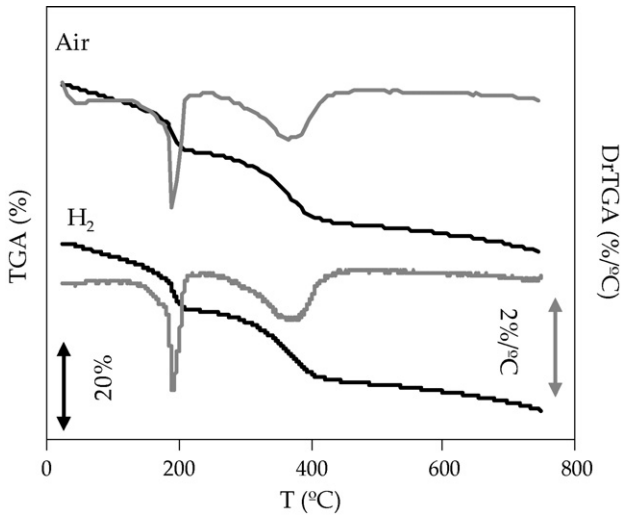

Fig. 2. TGA for HT precursor decomposition in air and hydrogen atmospheres.

temperature, the transition is a continuous loss of weight between 30 and 230 °C, which corresponds to the loss of interlaminar water, without structure collapse. The second step, which occurs between 230 and 430 °C, corresponds to the irreversible dehydroxilation of the brucite-type layers coupled with loss of carbonates. In particular, under reducing atmosphere, the weight loss is also affected by the transition of Ni(II) to Ni^0, with consequent loss of water [26].

Surface area (S_g) results as a function of calcination temperature are reported in Table 1. S_g of calcined samples (ex-HT-CX) is significantly greater than that of the precursor. It is known that, the release of water vapor and CO_2 through the LDH layers causes the solid craterisation process (pore formation) [26]. Surface area increases as temperature increases until a maximum close to 400 °C, and then a further increase in the calcination temperature produces a diminution of surface area. As it has been reported [27], samples calcined at temperatures in the range of decomposition temperature show a maximum value of S_g and it decreases with further calcination temperature increasing.

For the solid activated by direct reduction (ex-HT-R) no S_g increase respect the precursor is observed. It is possible that, as during direct activation both calcination and reduction processes coexist with the water evolution, a competence is set between them, favouring controlled elimination of volatile compounds, and thus avoiding solid craterisation [28].

In Figs. 3 and 4 PXRD patterns for calcined and reduced samples, respectively, are shown. During thermal decomposition in oxidizing atmosphere, the initial structure collapses (ex-HT-CX) because of the loss of carbonates (decarboxilation) and oxhydriles (dehydration), transforming the solid into an oxide mixture. The samples ex-HT-CX patterns show characteristic reflections of NiO (Bunsenite, JCPDS 22-1189); although MgO (JCPDS 4-0829) has a similar structure, NaCl-type, observed reflections at high angles centred in 2θ: 74.67 and 75.43 are consistent with NiO lattice

Table 1
Surface areas of the samples.

Sample	S_g (m^2/g)
HT	65.6
ex-HT-C300	133.9
ex-HT-C400	226.5
ex-HT-C500	188.4
ex-HT-C700	157.6
ex-HT-R	68.9
ex-HT-C700R	147.3

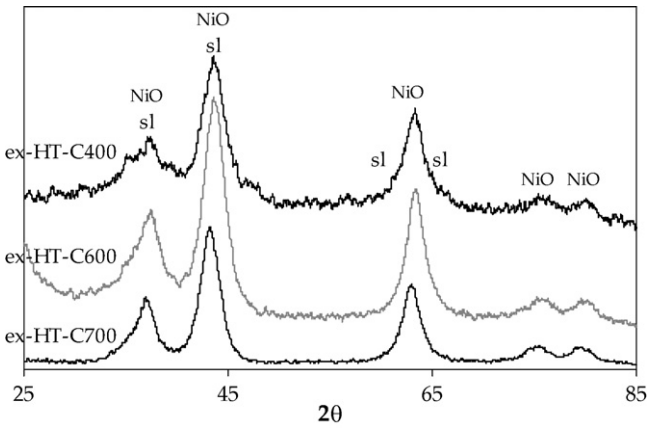

Fig. 3. PXRD patterns for calcined samples. (NiO): NiO; (sl): spinel-like phase.

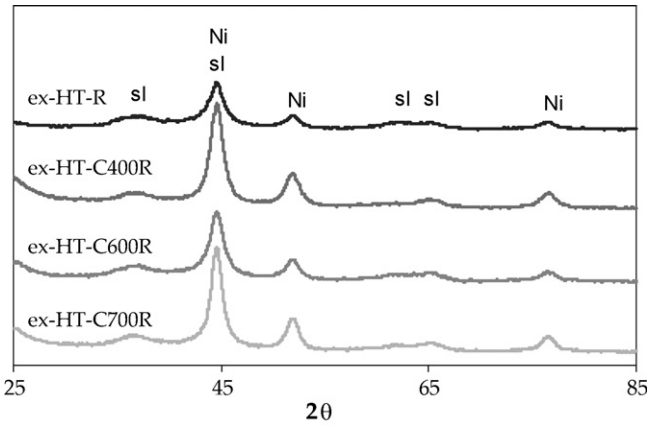

Fig. 4. PXRD patterns for reduced samples. (Ni):$Ni^{(0)}$; (sl): spinel-like phase.

parameter. After reducing step, in all samples (ex-HT-CXR), this phase evolves into metallic nanocrystalline Ni (JCPDS 4-0850); the low intensity reflections observed at 2θ: 31.3, 59.5 and 65.3° suggest the presence of a spinel-like phase (JCPDS 10-0339 $NiAl_2O_4$, 21-1152 $MgAl_2O_4$), in which the non-reducible Mg(II) and Al(III) ions remain.

Previous works based on neutron diffraction studies indicate that such mix phases crystallize in an incipient way at 650 °C [28], and massive segregation of this phase at temperatures close to 1000 °C is observed [29].

In the case of the one-step activated sample (ex-HT-R), it can be observed the presence of metallic Ni instead of NiO, coexisting with the weak reflections of the spinel-like phase.

Temperature programmed reduction (TPR) profiles (Fig. 5) obtained for the HT and ex-HT-CX samples indicate that reduction

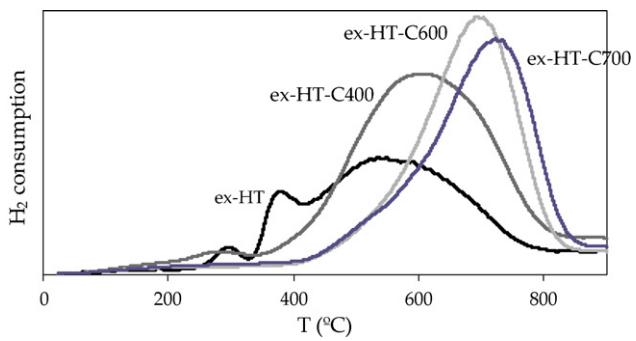

Fig. 5. TPR profiles for samples calcined at different temperatures.

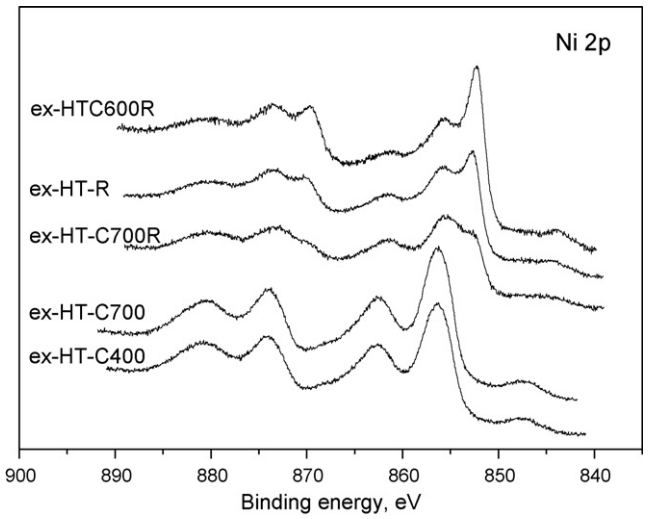

Fig. 6. XPS spectra of the Ni 2p core-level for the activated samples.

occurs in a wide temperature range associated to Ni(II) oxidic forms present in the samples [30]. The highest hydrogen consumption was obtained at 550 °C for the non-calcined sample (HT) and at 725 °C for the one treated at 700 °C (ex-HT-C700). The TPR maximum shifts to higher temperatures as well as the calcination temperature increases. This is related to a higher interaction between nickel atoms and the neighbouring cations [31].

In this regard, other researches [32,33] identified different Ni-species in alumina-supported catalyst assigning reduction peaks between 700 and 1000 °C to Ni(II)-spinel-type phases. On the other hand, the signals at 300 and 400 °C in HT sample can be assigned to pure NiO [33,34]. Quantitative analysis of the TPR profiles showed that in all samples about 94 ± 3% of the Ni content was reduced.

Fig. 6 shows XPS spectra of the Ni 2p core-level for the activated samples. Calcined samples present a main peak of Ni $2p_{3/2}$ centred in 856.0 eV with a shake-up satellite peak at 862.3 eV and the Ni $2p_{3/2-1/2}$ splitting of 17.6 eV. This indicates the presence of Ni(II) species in strong interaction with the support [34,35] suggesting the presence of surface ions Ni(II) in nickel spinel-like entities after air calcination. This figure also shows the spectrum corresponding to reduced samples: ex-HT-C700R, ex-HT-C600R and ex-HT-R. It must be noted that the samples were reduced *ex situ* following the protocol described in Section 2 and *in situ* in the pre-chamber XPS equipment, directly connected to the spectra acquisition chamber in order to revert the atmosphere oxidation of surface metallic nickel species suffered during sample handling.

Reduced sample spectra show after deconvolution for the three samples, binding energies for Ni $2p_{3/2}$ centred in the range of 852.4–852.6, 855.3–855.7 and 861.0–861.3 eV. These binding energies can be assigned to Ni^0, Ni^{2+} species in strong interaction with Al(III)-based support and Ni shake-up satellite, respectively. This fact indicates that the surface of the samples is not completely reduced after the reduction treatment. However, the samples show different Ni^0/Ni^{2+} surface ratios. For directly reduced (ex-HT-R) and for calcined at 600 °C and reduced (ex-HT-C600R) samples this ratio is close to 1, meanwhile for the sample ex-HT-C700R this ratio decreases to 0.5 as it is reported in Table 2. This table also reports surface molar fractions for cations and its comparison with bulk ratios for the precursor. It can be seen that calcination of the HT sample increments the surface aluminium species concentration, which reflects the massive cations redistribution driven by calcination. Similar results have been reported by Rebours et al. [36], who found surface enrichment of aluminium species after calcination of Ni(II)–Al(III) and Mg(II)–Al(III) LDHs. Our results show that, whatever is the activation method: calcination and reduction in two steps (ex-HT-CXR) or direct reduction (ex-HT-R), cations ratio in the surface is practically the same. Nevertheless, it must be noted that for samples ex-HT-R and ex-HT-C600R the Ni^0/Ni^{2+} surface ratio is twice the one obtained for the sample ex-HT-C700R.

Table 2
Surface molar fraction of the species and bulk composition for HT precursor. First line represents bulk data.

Sample	Al/ (Ni + Mg + Al)	Ni/ (Ni + Mg + Al)	Mg/ (Ni + Mg + Al)	$Ni^0/Ni^{2+}\|_{sup}$
HT bulk	0.35	0.51	0.14	–
ex-HT-C400	0.50	0.38	0.13	–
ex-HT-C600	0.50	0.36	0.13	–
ex-HT-C700	0.53	0.32	0.14	–
ex-HT-R	0.60	0.16	0.23	1.02
ex-HT-C600R	0.61	0.17	0.21	1.05
ex-HT-C700R	0.63	0.13	0.23	0.53

The catalysts were evaluated in the reaction of ethanol steam reforming in chemical control conditions analyzing the performance in stationary state (Table 3). Conversion and products yield were defined as follows: $x = (y^0_{EtOH} - y^s_{EtOH})/y^0_{EtOH}$; $Yi = (y^s_i - y^0_i)/y^0_{EtOH}$. The experiments were performed at the same space time, temperature and feed composition, in order to compare the ethanol conversions. It can be observed that both, exHT-R and exHTC600-R, present the higher ethanol conversion. In all cases the product distribution is related to the activity. When ethanol conversion increases, final products yield (H_2, CO and CO_2) increases, while the intermediate products yield (ethylene and acetaldehyde) decreases.

In Table 4, results of the kinetic evaluation using ex-HT-R, ex-HT-C600R and ex-HT-C700R catalysts, are compared with the metallic Ni area values determined by H_2 chemisorption and the Ni^0/Ni^{2+} surface molar ratio obtained by XPS.

As we mentioned above the ex-HT-R and ex-HT-C600R catalyst conversion and H_2 production are similar, while for ex-HT-C700R catalyst, those values fall almost to a half. This behaviour agrees with the values of metallic Ni areas and with the Ni^0/Ni^{2+} surface ratio obtained by XPS, suggesting that the catalytic activity per Ni atom (turnover) would be similar in all samples. The different behaviour lies in the fact that the number of reduced active sites (Ni^0) is higher, approximately twice, in the case of the directly reduced and calcined at 600 °C and reduced samples.

Table 3
Ethanol conversion and products yield.

Sample	Ethanol conversion	H_2 yield	CO yield	CO_2 yield	CH_4 yield	C_2H_4 yield	C_2H_4O yield
exHT-R	0.87	4.10	0.36	0.50	0.02	0.002	0.05
exHT-C300R	0.60	3.03	0.23	0.38	0.01	0.004	0.08
exHT-C400R	0.48	2.36	0.16	0.30	0.01	0.005	0.1
exHT-C500R	0.53	2.58	0.14	0.29	0.01	0.01	0.08
exHT-C600R	0.86	3.98	0.32	0.46	0.03	0.002	0.06
exHT-C700R	0.44	2.00	0.12	0.27	0.01	0.01	0.08

Table 4
Conversion and H_2 yield obtained in catalytic evaluation, Ni-metallic area obtained by H_2 chemisorption and $Ni^0/Ni^{2+}|_{sup}$ ratio obtained by XPS.

Sample	Ethanol conversion (%)	Yield to H_2 (%)	$Ni^0/Ni^{2+}|_{surf.}$	A_{Ni} (m^2/g)
exHT-R	87	68	1.02	23.6
exHT-C600R	86	66	1.05	22.3
exHT-C700R	44	33	0.53	12.0

During the thermal decomposition of carbonate forms of LDHs, a massive final dehydroxilation–decarboxilation step results in the pure oxidic form. However, due to the ratio of trivalent to divalent cations present in the matrix, a complex phase segregation process starts, in which the involved cations redistribute in order to reach their correspondent stable, commonly stoichiometrical, oxides [37–39]. The rate of segregation and the observed intermediate phases are strongly dependant on the nature of the involved cations; in the particular case of the ternary Ni(II)–Mg(II)–Al(III) LDHs, the starting oxide can be described as an ill crystallized spinel-like phase, in which all the cations share a single cubic oxygen framework. While Mg(II) and Al(III) can occupy either tetrahedral or octahedral positions within it, Ni(II) cations are exclusively placed at octahedral ones, irrespective of the Ni(II) to Mg(II) ratio [28]. With further calcination, the parent spinel-like metastable phase splits into two stable phases (demixing), and the segregation of crystalline NiO and $Ni_{1-x}Mg_xAl_2O_4$ spinel takes place, since Mg(II) cations preferentially accumulate in the latter phase [40,19]. In the present case, the stoichiometry of decomposition/demixing is depicted by Eqs. (2) and (3).

Decomposition

$$Ni_{0.51}Mg_{0.14}Al_{0.35}(OH)_2(CO_3)_{0.17}\cdot nH_2O \rightarrow \text{sl-}Ni_{0.51}Mg_{0.14}A_{l0.35}O_{1.17} + 0.17CO_2 + (1+n)H_2O \quad (2)$$

Demixing

$$\text{sl-}Ni_{0.51}Mg_{0.14}Al_{0.35}O_{1.17} \rightarrow 0.49NiO + 0.17Ni_{0.12}Mg_{0.88}Al_2O_4 \quad (3)$$

Previous reports indicate that the second reaction can be expected to be valid at temperatures close to 700 °C [41]. In parallel to the aforementioned structural and compositional changes, the decomposition process exerts dramatic textural changes over the parent material; the less abundant growing spinel phase migrates towards the surface of the already formed NiO-type particles in which the divalent cations naturally concentrate. After a proper thermal treatment this process ends in the "decoration" of the more abundant NiO particles with a shell of smaller $Ni_{0.12}Mg_{0.88}Al_2O_4$ ones [36]. Then, the observed XPS signal of the studied mixed oxides is strongly influenced by the latter phase. Following this consideration, Fig. 7 depicts the surface composition of the whole sample, assuming that the overall XPS signal obeys to the contribution of a pure NiO core increasingly masked by a $Ni_{0.12}Mg_{0.88}Al_2O_4$ shell. For those samples submitted to higher and/or longer thermal treatments (700 °C), the observed XPS signal can be described, in good agreement by the proposed model, assuming that the spinel covers a 90% of the sample's surface. However, for the samples treated at lower temperatures, the observed XPS signal cannot be described by the core-shell model suggesting an unfinished segregation process.

In addition, due to the fact that Ni(II) ions included within the spinel are non-reducible under the employed conditions, the proportion of solids described by Eq. (3) predicts a low temperature reduction of the 96% of the total Ni(II) ions of the sample, in good agreement with observed values of 94 ± 3% determined by TPR analysis.

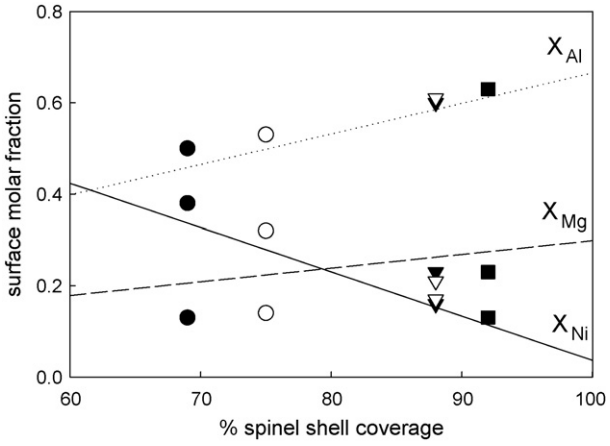

Fig. 7. Evolution of surface composition (X_{Ni} full line, X_{Mg} dashed line and X_{Al} dotted line) predicted by the core-shell model as a function of shell coverage percentage. Observed surface composition values for (●) ex-HT-C400; (○ ex-HT-C700; (▽) ex-HT-R; (▼) exHT-C600R; (■) ex-HT-C700R, overimposed to the most accurate value predicted by the model.

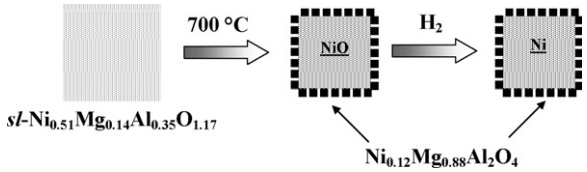

Scheme 1. Surface phase segregation model.

Scheme 1 illustrates the evolution of the process.

4. Conclusions

The Ni(II)–Mg(II)–Al(III) LDH obtained by homogeneous precipitation urea method, after a proper thermal treatment resulted in an active catalyst for the ethanol steam reforming. The results show that, whichever is the activation method: calcination at 600 °C and reduction at 720 °C (ex-HT-C600R) or direct reduction at 720 °C (ex-HT-R), the activity in ethanol steam reforming is the same, in agreement with chemisorption and XPS studies. Calcinations in air of a Ni(II)-rich LDHs develops a Ni(II)-poor spinel-type shell onto the NiO domains, evidenced by an increase in the surface Al(III) concentration. The reductive treatment results in an almost quantitative transformation of the NiO phase into Ni metallic crystallites highly dispersed in a stable Mg(II)–Al(III) matrix.

It can be seen from this report that the application on an appropriated activation treatment would allow to control the interaction of the Ni^0 active centres with the environment and the solid texture, redounding in an improved activity.

Acknowledgements

To ANPCyT, CONICET and UBA, for the economic support. Also, thanks are given to ANPCyT for Grant PME 8-2003 to finance the purchase of the UHV Multi Analysis System. MJ also acknowledge CONICET for the PIP 5215 project financial support.

References

[1] J. Comas, F. Mariño, M. Laborde, N. Amadeo, Chem. Eng. J. 98 (1–2) (2004) 61.
[2] F. Mariño, E. Cerrella, S. Duhalde, M. Jobbágy, M. Laborde, Int. J. Hydrogen Energy 23 (1998) 1095.
[3] S. Cavallaro, Energy Fuels 14 (2000) 1195.

[4] S. Freni, N. Mondillo, S. Cavallaro, G. Cacciola, V. Parmon, V. Sobyanin, React. Kinet. Catal. Lett. 71 (1) (2000) 143.
[5] J. Llorca, N. Homes, J. Sales, P. Ramírez de la Piscina, J. Catal. 209 (2002) 306.
[6] F. Mariño, G. Baronetti, M. Jobbágy, M. Laborde, Appl. Catal. A: Gen. 238 (2003) 41.
[7] J. Llorca, P. Ramírez de la Piscina, J.A. Delmon, J. Sales, N. Homes, Appl. Catal. B: Environ. 43 (2003) 355.
[8] S. Cavallaro, V. Chiodo, S. Freni, N. Mondillo, F. Frusteri, Appl. Catal. A: Gen. 249 (2003) 119.
[9] F. Aupretre, C. Descorme, D. Duprez, D. Casanave, D. Uzio, J. Catal. 233 (2005) 464.
[10] A. Akande, R. Idem, A. Delai, Appl. Catal. A: Gen. 287 (2005) 159.
[11] A. Haryanto, S. Fernando, N. Murali, S. Adhikari, Energy Fuels 19 (2005) 2098.
[12] S. Velu, K. Suzuki, M. Vijayaraj, S. Barman, C.S. Gopinath, Appl. Catal. B 55 (2005) 287.
[13] V. Mas, M.L. Dieuzeide, M. Jobbágy, G. Baronetti, N. Amadeo, M. Laborde, Catal. Today 133 (2008) 319.
[14] F. Frusteri, S. Freni, V. Chiodo, L. Spadaro, O. Di Biasi, G. Bonura, S. Cavallaro, Appl. Catal. A: Gen. 270 (2004) 1.
[15] J.R. Rostrup-Nielsen, J. Catal. 33 (1974) 184.
[16] F.V. Melo, N. Morlanés, Catal. Today 133–135 (2008) 374.
[17] J.R.H. Ross, M.C.F. Steel, A. Zeini-Isfahani, J. Catal. 52 (1978) 280.
[18] N.T. Dung, D. Tichit, B. Chiche, B. Coq, App. Catal. A: Gen. 169 (1998) 179.
[19] G.J. de, A.A. Soler-Illia, M. Jobbágy, R.J. Candal, A.E. Regazzoni, M.A. Blesa, J. Dispers. Sci. Technol. 19 (1998) 207.
[20] M. Jobbágy, M.A. Blesa, A.E. Regazzoni, J. Colloid Interface Sci. 309 (1) (2007) 72.
[21] N. Fairley, casaXPS Software, 2.3.13 Version, 2007-12-03.
[22] C. Wagner, A. Naumkin, A. Kraut-Vass, J. Allison, C. Powell, J. Rumble, NIST X-Ray Database 20, Version 3.4 (Web version). NIST Standard Reference database 20, National Institute of Standars and Tecnology, Gaintherburg, USA.
[23] V. Rives, M.A. Ulibarri, Coord. Chem. Rev. 181 (1999) 61.
[24] G.J. de, A.A. Soler-Illia, M. Jobbágy, A.E. Regazzoni, M.A. Blesa, Chem. Mater. 11 (1999) 3140.
[25] F. Cavani, F. Trifiró, A. Vaccari, Catal. Today 11 (1991) 173.
[26] O. Lebedeba, D. Tichit, B. Coq, Appl. Catal. A: Gen. 183 (1999) 61.
[27] K. Jirátová, P. Cuba, F. Kovanda, L. Hilaire, V. Pitchon, Catal. Today 76 (2002) 43.
[28] M. Gazzano, W. Kagunya, D. Matteuzzi, A. Vaccari, J. Phys. Chem. B 101 (23) (1997) 4514.
[29] O. Clause, M. Gazzano, F. Trifirò, A. Vaccari, L. Zatorski, Appl. Catal. 73 (2) (1991) 217.
[30] J. Rodriguez, J. Hanson, A. Frenkel, J. Kim, M. Perez, J. Am. Chem. Soc. 124 (2002) 346.
[31] T. Tichit, F. Medina, B. Coq, R. Dutartre, Appl. Catal. A: Gen. 159 (1997) 241.
[32] B.W. Hoffer, A. Dick van Langeveld, J.P. Janssens, R.L.C. Bonné, C.M. Lok, J.A. Moulijn, J. Catal. 192 (2000) 432.
[33] B. Scheffer, P. Molhoek, J.A. Moulijn, Appl. Catal. 46 (1989) 11.
[34] L. Dussault, J. Dupin, C. Guimon, M. Monthioux, N. Latorre, T. Ubieto, E. Romeo, C. Royo, A. Monzón, J. Catal. 251 (2007) 223.
[35] R. Guil-López, V. La Parola, M. Peña, J.L.G. Fierro, Catal. Today 116 (2006) 289.
[36] B. Rebours, J. d'Espinose de la Caillerie, O. Clause, J. Am. Chem. Soc. 116 (1994) 1707.
[37] M. Bellotto, B. Rebours, O. Clause, J. Phys. Chem. 100 (20) (1996) 8527.
[38] M. Bellotto, B. Rebours, O. Clause, J. Phys. Chem. 100 (20) (1996) 8535.
[39] E. Sileo, M. Jobbágy, C. Paiva-Santos, A. Regazzoni, J. Phys. Chem. B 109 (2005) 10137.
[40] F. Basile, L. Basini, M. D'Amore, G. Fornasari, A. Guarinoni, D. Matteuzzi, G. Del Piero, F. Trifirò, A. Vaccari, J. Catal. 173 (1998) 247.
[41] O. Clause, B. Rebours, E. Merlen, F. Trifirò, A. Vaccari, J. Catal. 133 (1992) 231.